Check for updates

An effective fluorescent sensor for lipopolysaccharide-induced H2S detection and imaging in inflammatory cells, zebrafish, and mouse blood samples†

Xinrong Zou,‡[abcd] Meiling Pang,‡[e] Jun He,[e] Zhuxi Kang,[f] Gulixiayida Wumaier,[d] Shenglai Xue[d] and Lingli Yuan 🄳 *[abc]

In this work, a new fluorescent sensor (NAHCP) for the recognition of lipopolysaccharide-induced H2S detection and imaging in inflammatory Raw264.7 cells, zebrafish, and mouse blood samples was constructed. Based on the *o*-aldehyde group (*o*-CHO) auxiliary 2,4-dinitrophenyl ether (DNP) group sulfide cleavage, this sensor shows high sensitivity and selectivity towards H2S, which can realize fluorescence "turn-on" detection. This sensor also features a very high response speed (∼2 min) and a large Stokes shift (113 nm) toward H2S. Additionally, the excellent detection limit (LOD) for H2S is as low as 25.6 nM. Impressively, this *o*-CHO auxiliary DNP group sulfide cleavage ensemble is further successfully applied for H2S detection in inflammatory Raw264.7 cells, zebrafish, and mouse blood samples.

1 Introduction

Inflammation is a basic physiological and pathological process of the body. When the body's living tissues are stimulated by certain exciting or damaging factors (such as trauma, infection, *etc.*), the body's defense response is the main manifestation of inflammation. Local manifestations of inflammation are redness, swelling, heat, pain, and functional disorders, accompanied by responses such as changes in the number of white blood cells, fever, and an immune response. Usually, inflammation is beneficial and is an automatic defense reaction of the organism. However, sometimes inflammation is also harmful (for example, attacking the organism's tissues, *etc.*). Modern biological medicine shows that inflammation *in vivo* is

aDepartment of Hematology, The Second Xiangya Hospital, Central South University, Changsha, Hunan, 410011, PR China. E-mail: lingliestelle@csu.edu.cn; linglimonica@aliyun.com

bInstitute of Molecular Hematology, Central South University, Changsha, Hunan, 410011, PR China

cHunan Engineering Research Center of Cell Immunotherapy for Hematopoietic Malignancies, Changsha, Hunan, 410011, PR China

dThe Key Laboratory of Biochemistry and Molecular Pharmacology, College of Pharmacy, Chongqing Medical University, Chongqing, 400016, PR China

eThe Third Hospital of Mianyang, Sichuan Mental Health Center, The Affiliated Mianyang Hospital of Chongqing Medical University, Mianyang, Sichuan 621000, PR China
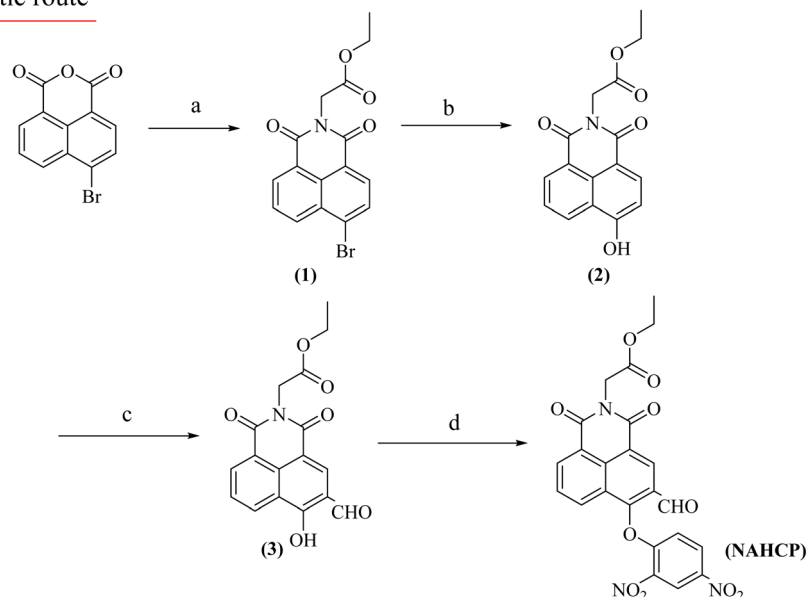
fSinopharm Dongfeng General Hospital, Hubei University of Medicine, Shiyan, Hubei 442008, PR China

† Electronic supplementary information (ESI) available. See DOI: https://doi.org/10.1039/d5ra03905c

‡ Equal contribution authors (X. Zou and M. Pang).

inseparably associated with the occurrence and development of some diseases. Inflammation usually produces related biomarkers, and the detection of inflammation-related biomarkers is of great significance for the diagnosis of some diseases. While hydrogen sulfide (H2S) is a highly relevant gas signal molecule,[1–5] it has attracted great interest from scientific researchers. Recent studies have shown that endogenous H2S participates in a series of physiological processes.[6–11] In addition, the abnormal expression of endogenous H2S levels in biological systems was considered to be closely associated with the occurrence and development of various diseases,[12–16] thus, H2S is usually considered to be related to the occurrence and development of inflammation and can be used as a biomarker is commonly used as a biomarker for these diseases diagnosis. In general, H2S is produced from L-cysteine (Cys) catalyzed by a variety of important enzymes and converted into a variety of sulphur-containing compounds.[17] Although current studies have shown that H2S is related to the occurrence and development of many physiological and pathological processes, the specific molecular mechanisms of H2S are still unclear. Therefore, it is important and urgently needed to develop molecular tools with high selectivity, high sensitivity, and high biocompatibility to monitor the occurrence and development of H2S and inflammation in complex biosystems.

With the continuous update of detection methods and tools, many tools and methods for H2S have been developed in recent years. To our dismay, these methods cannot achieve H2S non-invasive, *in situ*, and real-time monitoring in biosystems.[18] In contrast, fluorescence sensor methods based on small molecule fluorescent dyes have been extensively investigated by scientific
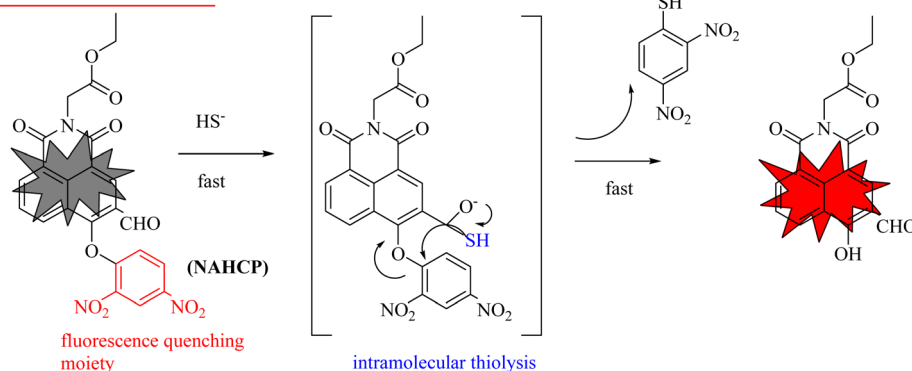
Synthetic route

Sensing Mechanism

Fig. 1 Schematic diagram of the synthesis route and sensing mechanism of NAHCP: (a) glycine ethyl ester hydrochloride, triethylamine, EtOH, 40 °C, 4 h; (b) N-hydroxyphthalimide, K_2CO_3, and DMF, 110 °C, 2 h; (c) hexamethylenetetramine and F_3CCOOH, 80 °C, 4 h; (d) 2,4-dinitro-fluorobenzene and triethylamine, RT, 3 h.

researchers for their potential advantages, for example, simplicity, high sensitivity, high selectivity, fast reaction time, real-time monitoring, and *in situ* non-invasive visualization,[19–22] meanwhile, the performance of some latest H_2S sensors was summarized and a simple comparison with this work (Table S1†). Therefore, in recent years, by designing and screening excellent sulfide-responsive moieties through the unique chemical properties of H_2S,[23–26] which respond to H_2S. Despite the remarkable achievements in recent years, such as the current fluorescent probe for H_2S based on azide reduction, nitro reduction, DNP and NBD cleavage, and disulfide cleavage (Table S1†), there are still some defects that need to be overcome to meet the needs of application requirements (such as poor selectivity, poor stability, long response time, small Stokes shift, *etc.*). To overcome these limitations, there is an urgent need for small-molecule H_2S sensors with high sensitivity and high selectivity, fast response, excellent optical performance, and high biocompatibility.

Based on the above requirements, according to the literature report,[27,28] the *o*-CHO as the auxiliary group has better selectivity and fast response toward H_2S. Thus, this work adopts the dual-parental nucleophilicity of H_2S, construction of a new fluorescent sensor NAHCP (Fig. 1) for H_2S detection and visualization in living cells, zebrafish, and blood samples. NAHCP was introduced into a selected naphthylimide with good optical performance and biocompatibility as the fluorophore, and an *o*-aldehyde group auxiliary 2,4-dinitrophenyl ether group as the response site and as the fluorescence quencher group to achieve highly specific detection of H_2S in biosystems. After the nucleophilic substitution reaction between H_2S and the double recognition, the cascade reaction is triggered to release the naphthylimide fluorophore, which has a good intramolecular electron transfer (ICT) effect, the naphthylimide itself emits a strong fluorescence signal, and then the fluorescence "Off–On" recognition of H_2S is realized. In addition, NAHCP could be applied for fluorescence visualization of H_2S in living LPS-induced Raw264.7 cells, zebrafish, and blood samples of mice.

2 Experimental part

2.1 Apparatus and reagents

2.1.1 Apparatus. LCQ Fleet mass spectrometer (MS, Thermo Fisher Scientific, USA), DPX-400 nuclear magnetic resonance (DMSO-d_6 as solvent, TMS as an internal standard, Bruker, Germany), G9800A fluorescence spectrophotometer (Agil, USA), UV-2700 ultraviolet-visible spectrophotometer (UV-Vis, Shimadzu, Japan), WIGGENSWCI-1802 constant temperature incubator (Beijing Sandeyi Experimental Instrument Research Institute, China), FV1200 laser confocal microscope (Olympus, Japan).

2.1.2 Reagents. Dichloromethane, ethanol, anhydrous sodium sulfate (Na$_2$SO$_4$), sodium chloride (NaCl), petroleum ether, and ethyl acet were all purchased from the National Pharmaceutical Group Chemical Reagent Co., Ltd (China), 4-bromo-1,8-naphthalic anhydride (CAS: 81-86-7), glycine ethyl ester hydrochloride (CAS: 623-33-6), N-hydroxyphthalimide (CAS: 524-38-9), 2,4-dinitrofluorobene (CAS: 70-34-8), hexamethylenetetramine (CAS: 100-97-0), trifluoroacetic acid, and anhydrous potassium carbonate were all purchased from J&K Scientific. Experimental water was deionized water. Raw264.7 cells (Chongqing Medical University). The all reagents used do not need to be purified and can be used directly.

2.2 Synthesis of NAHCP

2.2.1 Synthesis of compound 1. Compound **1** was synthesized according to the method reported in the literature with slight modification.[29] In N$_2$ protection, 4-bromo-1,8-naphthalic anhydride (10 mmol, 2.77 g), glycine ethyl ester hydrochloride (10 mmol, 1.04 g), and triethylamine (5 mL) were in a reactor with anhydrous ethanol (30 mL), heated at 40 °C for 4 h, and then the reaction system has cooled to room temperature (RT), the solid was filtered and dried, obtaining a white solid **1** (2.90 g, 80.1%), and the resulting solid does not need to be purified, and can be used directly for the next step of synthesis.

2.2.2 Synthesis of compound 2. **2** was carried out based on of the method reported in the literature.[30] Compound **1** (5 mmol, 1.81 g), N-hydroxyphthalimide (10 mmol, 1.63 g), and K$_2$CO$_3$ (15 mmol, 2.07 g) were dissolved in a reactor with N,N-dimetylformamide (30 mL, DMF) under N$_2$ protection. The reaction system was heated at 110 °C for 120 min, and then added into ice-water after the reaction system had cooled to RT. At this time, a large amount of solid was generated. After standing for 60 min, a yellow solid **2** was obtained by filtering and dried (1.10 g, 74.8% yield). ^{1}H NMR (400 MHz, DMSO-d_6),δ (ppm): 10.04 (s, 1H), 8.58 (d, J = 8.00 Hz, 1H), 8.50 (d, J = 8.00 Hz, 1H), 8.38 (d, J = 8.00 Hz, 1H), 7.79 (t, J = 8.00 Hz, 1H), 7.19 (d, J = 8.00 Hz, 1H), 4.78 (s, 2H), 4.16 (dd, J = 8.00 Hz, 2H), 1.21 (t, J = 8.00 Hz, 3H); ^{13}C NMR (100 MHz, DMSO-d_6),δ (ppm): 168.67, 163.87, 163.08, 161.28, 134.55, 123.06, 129.99, 129.78, 126.26, 122.96, 121.66, 112.36, 110.64, 61.49, 55.44, 14.51.

2.2.3 Synthesis of compound 3. Compound **3** was synthesized according to the method reported in the literature with slight modification.[31] Compound **2** (2.5 mmol, 0.75 g) and hexamethylenetetramine (2.5 mmol, 0.35 g) were dissolved in a reactor with trifluoroacetic acid (30 mL) under N$_2$ protection, heated at 80 °C for 4 h, and then the trifluoroacetic acid was evaporated by rotary evaporation. Finally, a yielding yellow solid **3** (0.62 mg, 75.2% yield) was purified by flash column chromatography with dichlorometh: methanol = 20 : 1 as the eluent. ^{1}H NMR (DMSO-d_6, 400 MHz),δ (ppm): 12.18 (s, 1H), 10.30 (s, 1H), 8.80 (s, 1H), 8.30 (d, J = 24.00 Hz, 2H), 7.35 (s, 1H), 4.81 (s, 2H), 3.50 (dd, J = 8.00 Hz, 2H), 1.11 (t, J = 4.00 Hz, 3H); ^{13}C NMR (DMSO-d_6, 100 MHz) δ (ppm): 174.66, 169.11, 164.35, 162.81, 136.65, 132.13, 131.97, 131.40, 127.10, 122.80, 121.07, 115.36, 101.93, 61.25, 54.93, 14.54.

2.2.4 Synthesis of NAHCP. NAHCP was synthesized according to the method reported in the literature with slight modification.[32] 0.50 g compound **3** (1.53 mmol), 0.285 g 2,4-dinitrofluorobenzene (1.53 mmol), and 2 mL triethylamine were dissolved in a reactor (50 mL) with dichloromethane (DCM) under N$_2$ protection. The mixture was allowed to proceed at room temperature for 3 h, and after removal of DCM, the crude product was purified by quick column chromatography with DCM as the eluent to obtain a yellow solid (0.642 mg, 85.2% yield). ^{1}H NMR (400 MHz, DMSO-d_6), δ (ppm): 9.49 (s, 1H), 8.85 (d, J = 4.00 Hz, 1H), 8.78 (d, J = 8.00 Hz, 1H), 8.47 (d, J = 8.00 Hz, 2H), 8.21 (dd, J = 4.00 Hz, 1H), 7.83 (t, J = 8.00 Hz, 1H), 7.16 (d, J = 8.00 Hz, 1H), 4.75 (s, 2H), 4.13 (dd, J = 8.00 Hz, 2H), 1.19 (t, J = 8.00 Hz, 3H); ^{13}C NMR (100 MHz, DMSO-d_6), δ (ppm): 168.58, 163.69, 162.97, 158.54, 148.34, 135.69, 133.40, 131.81, 130.61, 130.05, 129.08, 126.57, 124.08, 123.57, 121.76, 120.83, 115.69, 112.85, 61.51, 55.37, 14.48. HRMS characterization of NAHCP ([C$_{23}$H$_{15}$N$_3$O$_{10}$]), calculated: 493.0757; found: 493.0758.

2.3 Spectral test

2.3.1 Optical physical property test. Take an appropriate amount of NAHCP to dissolve in DMSO to obtain a pure NAHCP DMSO stock solution of 10 mM. The above solution was diluted to 10 μM with 10 mM PBS, and scanned under UV-Vis and fluorescence spectrophotometry to determine the absorption spectrum, fluorescence emission spectrum, and to determine the maximum absorption wavelength, fluorescence emission wavelength, and other optical physical property parameters. H$_2$S was generated by the hydrolysis of Na$_2$S dissolved in water, and was prepared on the spot. Weigh the corresponding mass of each potential competitive substance, and dissolve dilute it with PBS solution (Blank, Na$_2$S, K$^+$, Ca^{2+}, Mg^{2+}, Hg^{2+}, Zn^{2+}, Cu^{2+}, Fe^{3+}, Cr^{3+}, SCN$^-$, NO$_3^-$, SO$_4^{2-}$, SO$_3^{2-}$, CO$_3^{2-}$, ClO$^-$, Ac$^-$, H$_2$PO$_4^-$, H$_2$O$_2$, Cys, and GSH). The concentration of NAHCP used was 10 μmol L^{-1}. The kinetic measurement of NAHCP reaction: 100 μM Na$_2$S was taken and added to NAHCP of DMSO solution (10 μM), respectively, and stirred, and its fluorescence intensity was measured at 0, 10, 20, 30, 40, 50, 60, 70, 80, 90, 100, 110, 120, 130, 140, 150, 160, 170, 180, 190, and 200 s, respectively. Titration experiment of NAHCP: H$_2$S (0–100 μM) solution was gradually added to 10 μM NAHCP (pH = 7.4), and the fluorescence intensity at 533 nm was measured. The λ_{ex} was set at

420 nm, and the λ_{em} was fixed on 533 nm, and the λ_{ex} and λ_{em} slits were 5 nm, respectively. All testing was repeated 3 times ($n = 3$).

2.4 Cell fluorescence imaging experiment

Raw264.7 cells were placed in a culture medium containing fetal bovine serum and incubated at 37 °C and 5% CO_2. For cell imaging, log-phase Raw264.7 cells were seeded into confocal-specific culture dishes and cultured overnight in a constant temperature incubator to allow them to adhere to the wall. In the cytotoxicity experiment, after cell adherence, NAHCP stock solution was diluted with culture medium, and cells were cultured with different concentrations of NAHCP (0–30 μM) for 2 days, and the Raw264.7 cell survival was monitored by the MTT colorimetry. In the Raw 264.7 cell imaging experiment, the final concentration of NAHCP in the confocal culture dish was 10 μM, and the Raw264.7 cells were cultured for 30 min, washed with PBS three times, and images were taken without the addition of H_2S, images with the addition H_2S were taken to monitor the changes in fluorescence intensity in the living cells. In addition, for endogenous H_2S, the living Raw264.7 cells were stimulated by LPS (1 μg mL^{-1}) for 2 h, NAHCP was added, and then imaged and analyzed. $\lambda_{ex} = 420$ nm, $\lambda_{em}=(500–550)$ nm, scale bar 10 μm. All testing was repeated 3 times ($n = 3$).

2.5 Zebrafish fluorescent imaging experiment

Healthy zebrafish (48 h-old) were transferred to PBS and separated into three groups. Group 1 was the control group, which was exposed directly to a solution of PBS containing 10 μM NAHCP, and fluorescence imaging was performed after 30 min. Group 2 was cultured with H_2S solution (100 μM) for 0.5 h, next, the NAHCP was added and cultured for another 0.5 h, finally, the fluorescence images were performed after PBS washes 3×. Group 3 was induced with LPS (1 μg mL^{-1}) for 2 h, next, the NAHCP was added and cultured for another 0.5 h, finally, the fluorescence images were performed. $\lambda_{ex} = 420$ nm, $\lambda_{em}=(500–550)$ nm, scale bar 10 μm. All testing was repeated 3 times ($n = 3$).

2.6 Detection of H_2S in blood samples

Take LPS-induced Kunming mice (6–9 weeks), and obtain blood samples through the mouse eye. After simple centrifugation of the blood the serum was diluted with PBS, and then added with H_2S solution (100 μM) or without H_2S solution (0 μM), and the samples were diluted to 5 mL with PBS to obtain the test samples, and measure the fluorescence intensity of the solution with a fluorometer. The $\lambda_{ex} = 420$ nm, $\lambda_{em} = 533$ nm, and the
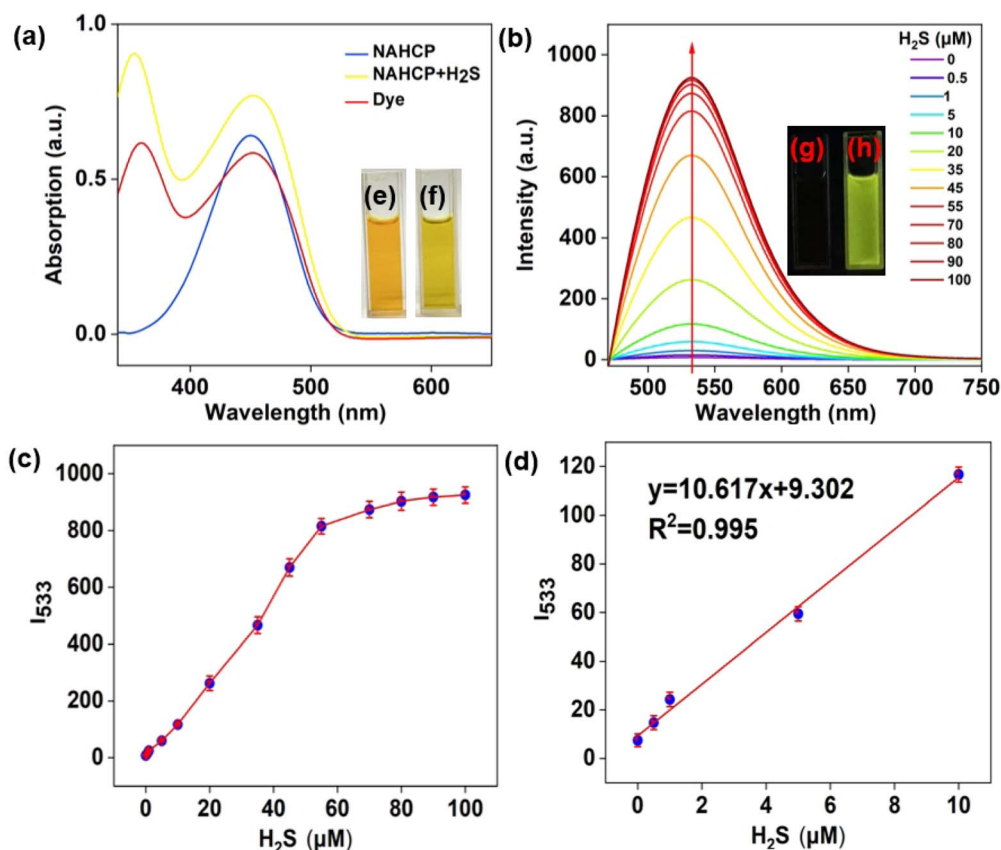

Fig. 2 Spectral response properties of NAHCP for H_2S. (a) UV-visible absorption spectra of 10 μM NAHCP, 10 μM dye **3**, and 10 μM NAHCP + 100 μM H_2S; (b) the fluorescence response spectrum of the 10 μM NAHCP toward different concentrations of H_2S (0–100) μM; (c) the fluorescence intensity of I_{533} change vs. different concentrations of H_2S (0–100) μM; (d) the I_{533} of the 10 μM NAHCP responded linearly to the range from 0 to 10 μM H_2S; (e and f) the bright-field imaging of 10 μM NAHCP in the absence and the presence of 100 μM H_2S, respectively, the embedding graph in picture (a); (g and h) the 365 nm UV-lamp radiated fluorescent imaging of 10 μM NAHCP in the absence and the presence of 100 μM H_2S, respectively, the embedding graph in picture (b). All detection systems in 10 mM PBS buffer (5% DMSO, v/v, pH 7.4) at 37 °C, $n = 3$.

excitation and emission slits were fixed on 5 nm, respectively. All testing was repeated 3 times ($n = 3$).

3   Results and discussion

3.1   Design and synthesis of the NAHCP

Because the fluorophore naphthylimine has some excellent optical properties, and some H_2S fluorescent probes have been constructed based it.[33,34] In this work, NAHCP was designed to use the fluorophore naphthylimine **3**, which comprises an *ortho*-aldehyde group (*o*-CHO) and a hydroxyl group (–OH), so that we can use the reported method in the literature with the Duff reaction to synthesize the *o*-CHO group.[31] By using the common response group precursor compound 1-fluoro-2,4-dinitrobenzene, the –OH can be simply protected to prepare NAHCP as shown in Fig. 1, which was prepared from the most initial raw 4-bromo-1,8-naphthalic anhydride through four-step reactions. The synthesis details can be found in Fig. 1, and the

NAHCP synthesized was characterized by NMR spectrometry (see ESI†), and the response mechanism was verified by mass spectra analysis (Fig. S2†).

3.2   Spectral properties of NAHCP

To investigate the optical characteristics and sensing capability of NAHCP, its UV-Vis absorption and fluorescence spectra were tested. The UV-Vis spectra of compound **3** and NAHCP were shown in Fig. 2a. Compound **3** has two significant absorption peaks at 350 nm and 420 nm, while NAHCP has only one maximum absorption peak at 350 nm, which is consistent with the position of the absorption peak of the compound **3** at the short wavelength, and NAHCP reacts with H_2S, two absorption peaks are generated simultaneously, which are consistent with the position of the absorption peak of compound **3**, and the color of the solutions changes from orange to yellow (Fig. 2e and f). Subsequently, the fluorescence reaction of NAHCP with H_2S was investigated. As shown in Fig. 2b, when the excitation
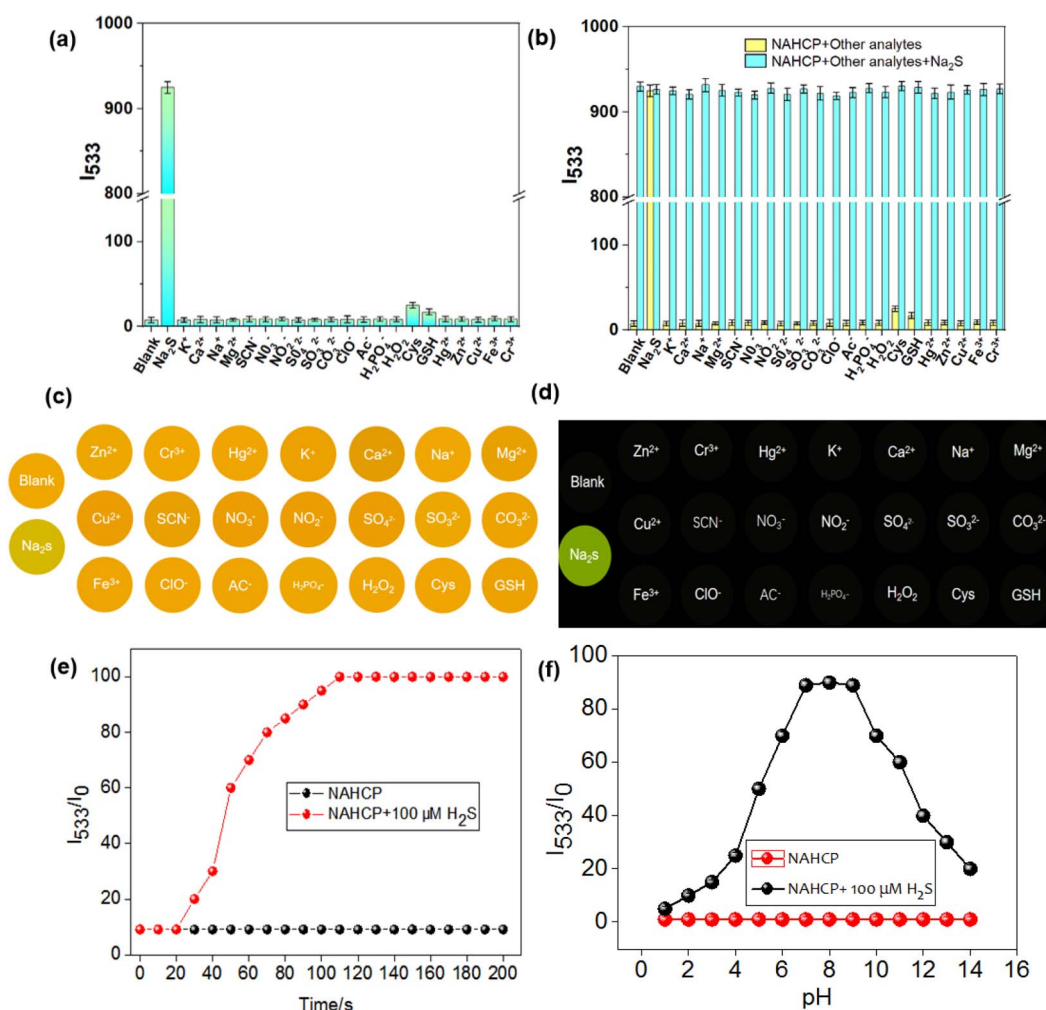

Fig. 3   The response performance studies of NAHCP toward H_2S. (a) The selectivity test; (b) the competitive experiment; (c and d) NAHCP for the response performance of various potential interferences on the silica gel plate, bright-field image and 365 nm UV-irradiated fluorescence image, respectively. (e and f) The fluorescence ratio changes (I_{533}/I_0) of NAHCP (10 μM) over time and pH in the absence (0 μM) or presence of H_2S (100 μM), $\lambda_{ex} = 420$ nm, $\lambda_{em} = 533$ nm, and the excitation and emission slits were 5 nm, respectively, $n = 3$.

wavelength is 420 nm, NAHCP has a significant emission band at 533 nm, and with the continuous increase of H_2S concentration (0–100 μM), the fluorescence intensity of NAHCP at 533 nm gradually increases. In addition, the fluorescence intensity ratio (I_{533}/I_0) is enhanced by ~100-fold, and the solution of the fluorescence color changes from colorless to bright green (Fig. 2g and h). In the range of H_2S concentration (0–10 μM), the fluorescence intensity I_{533} of NAHCP exhibited an outstanding linear relationship with the concentration of H_2S (Fig. 2d), $R^2 = 0.995$, and its detection limit is as low as 25.6 nM. As shown in Fig. 3b, when H_2S (100 μM) is added to 10 μM NAHCP (10 mM PBS solution, pH = 7.4, 37 °C), the response toward H_2S reaches the kinetic equilibrium within ~120 s, and all the above results showed that NAHCP can rapidly and effectively detect H_2S. Based on these spectroscopic data, NAHCP has the potential to achieve rapid, efficient, and highly sensitive detection of H_2S.

3.3 Response of NAHCP to H_2S and its anti-interference ability test

Selectivity is a key parameter to test the application ability of a sensor in complex environments. First, its specificity towards H_2S was verified by measuring NAHCP's response to biological thiols, related anions, cations, and other biological relevant analytes including Blanck, Na_2S, K^+, Ca^{2+}, Mg^{2+}, Hg^{2+}, Zn^{2+}, Cu^{2+}, Fe^{3+}, Cr^{3+}, SCN^-, NO_3^-, SO_4^{2-}, SO_3^{2-}, CO_3^{2-}, ClO^-, Ac^-, $H_2PO_4^-$, H_2O_2, Cys, and GSH. As shown in Fig. 3a, in the selectivity experiment, H_2S (100 μM) was added, the fluorescence intensity of NAHCP was significantly enhanced, whereas when the concentration of other relevant analytes was added, the fluorescence intensity of NAHCP remained almost unchanged, which indicated that NAHCP had good selectivity and sensitivity for H_2S compared to general interferents, and there was no significant enhancement of fluorescence intensity

for the interference with the thiol group. At the same time, in order to ensure that NAHCP can detect H_2S without interference in a complex system, a competitive test was carried out (Fig. 3b). The results showed that NAHCP can detect H_2S in complex conditions without interference, and has good response performance. In addition, to further confirm the specificity of NAHCP, firstly, the silica gel plate was soaked in 10 μM NAHCP solution and dried, subsequently, the analytes were dropped on the silica gel plate, and finally, take photos through the camera under brightfield and fluorescence field, the pictures were cut and assembled into the picture of Fig. 3c and d. It could be seen from the test results that only H_2S could cause color change (Bright-fields imaging, Fig. 3c) and fluorescence change (365 nm UV-activated fluorescence imaging, Fig. 3d). Finally, since all the above experiments were conducted for the detection of H_2S in living organisms in order to adapt to the normal pH value of living organisms, which is pH = 7.4, further research on the optimal detection pH was conducted (Fig. 3f). The experimental results showed that NAHCP responds to H_2S with a relatively wide pH range. The fluorescence ratio intensity (I_{533}/I_0) rapidly increased from pH = 1.0 to pH = 6.0, remained unchanged from pH = 6.0 to pH = 9.0, and rapidly decreased from pH = 9.0 to pH = 14.0. Therefore, all subsequent experiments were performed with a pH value of 7.4.

3.4 Cell imaging of NAHCP

Before fluorescence imaging, it is very necessary to investigate whether NAHCP has good biocompatibility and low toxicity. Therefore, Raw264.7 cells were cultured to evaluate the cytotoxicity of NAHCP to cells at different concentrations by the MTT method. The results are shown in Fig. S1,† the survival rate was above 85% even if the cells were incubated with a high concentration of 30 μM for 24 h. From this, it can be seen that NAHCP has low cytotoxicity, excellent biocompatibility, and can
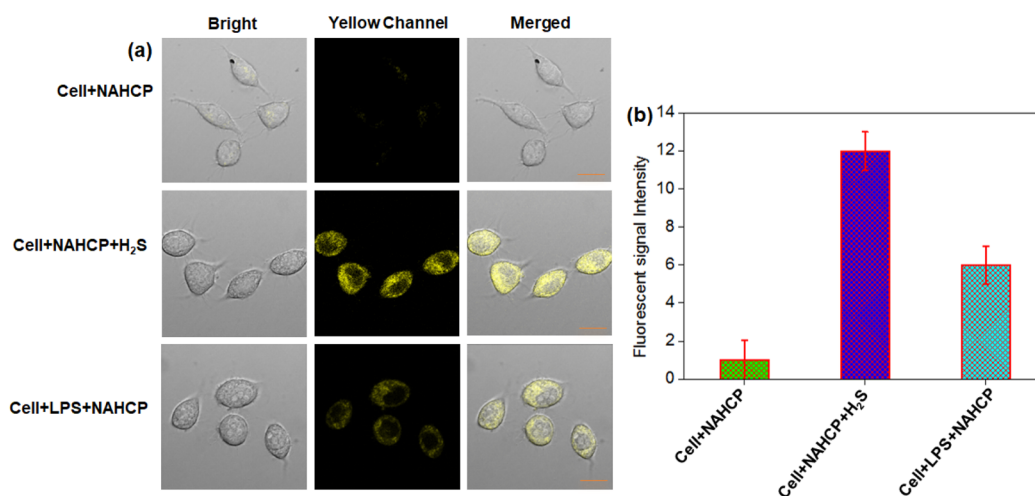

Fig. 4 (a) Laser confocal imaging of NAHCP (10 μM) in living Raw264.7 cells. Top row: the Raw264.7 cells were incubated with NAHCP (10 μM) for 30 min as the control group; middle row: the Raw264.7 cells were incubated with NAHCP (10 μM) for 30 min and then with H_2S 50 μM for 30 min; bottom row: the Raw264.7 cells were incubated with LPS (1.0 μg mL^{-1}) for 2 h and then with NAHCP (10 μM) for 30 min. (b) The quantitative analysis of the average fluorescence in the top row, middle row, and bottom row. λ_{ex} = 420 nm, λ_{em} = (520–550) nm, scale bar:10 μm, n = 3.

be used for cell imaging. Next, it is verified whether NAHCP can be used to detect changes in H₂S in living cells. The first group was imaged and analyzed after incubating with living cells for 30 min, and the cells only had a weak fluorescence signal in the yellow channel (Fig. 4: top row). In the second group, 100 μM H₂S was added to the culture medium that had been incubated with NAHCP for 30 min, and then imaged and analyzed after 30 min, and the cells emitted a bright yellow fluorescence signal in the yellow channel, indicating that Na₂S, as an explosive H₂S donor can quickly enter the cells and rapidly release H₂S, and further react with NAHCP to generate a dye **3** with strong fluorescence (Fig. 4: middle row). Finally, for the endogenous H₂S detected, we used LPS to stimulate the cells for 2 h, and then added NAHCP for imaging research, and found that the fluorescence intensity in the cells was stronger than in the blank control top row, indicating that NAHCP can detect endogenous H₂S in living cells (Fig. 4: bottom row). In addition, the quantitative analysis of the average fluorescence in the middle row and bottom row increases ∼12-fold and ∼6-fold. Therefore, the above excellent experimental results show that NAHCP can monitor H₂S in biological systems.

3.5 Imaging study of H₂S in zebrafish

Based on the above good experimental results, the ability of NAHCP for H₂S detection and imaging in zebrafish was investigated. As shown in Fig. 5a, in the control group (top row), after incubation of living zebrafish with 10 μM NAHCP solution at 37 °C for 30 min, there was a weak yellow fluorescence in the yellow channel. Next, in the experimental group (middle row), the zebrafish were first incubated with NAHCP (10 μM) at 37 °C for 30 min, and then incubated with 100 μM H₂S solution for 30 min, and then washed with PBS for imaging. It can be observed that in the yellow channel, there was a significant enhancement of the fluorescence signal. At last, also imaged with LPS to stimulate the zebrafish for 2 h, and then incubated with NAHCP for 30 min, the results showed that the fluorescence in the yellow channel was stronger than that in the control group, and weaker than that in the group with H₂S added (bottom row), and the corresponding normalized fluorescence intensity also verified this experimental (Fig. 5b). The above excellent experimental results show that NAHCP can image and monitor H₂S in complex biological systems.
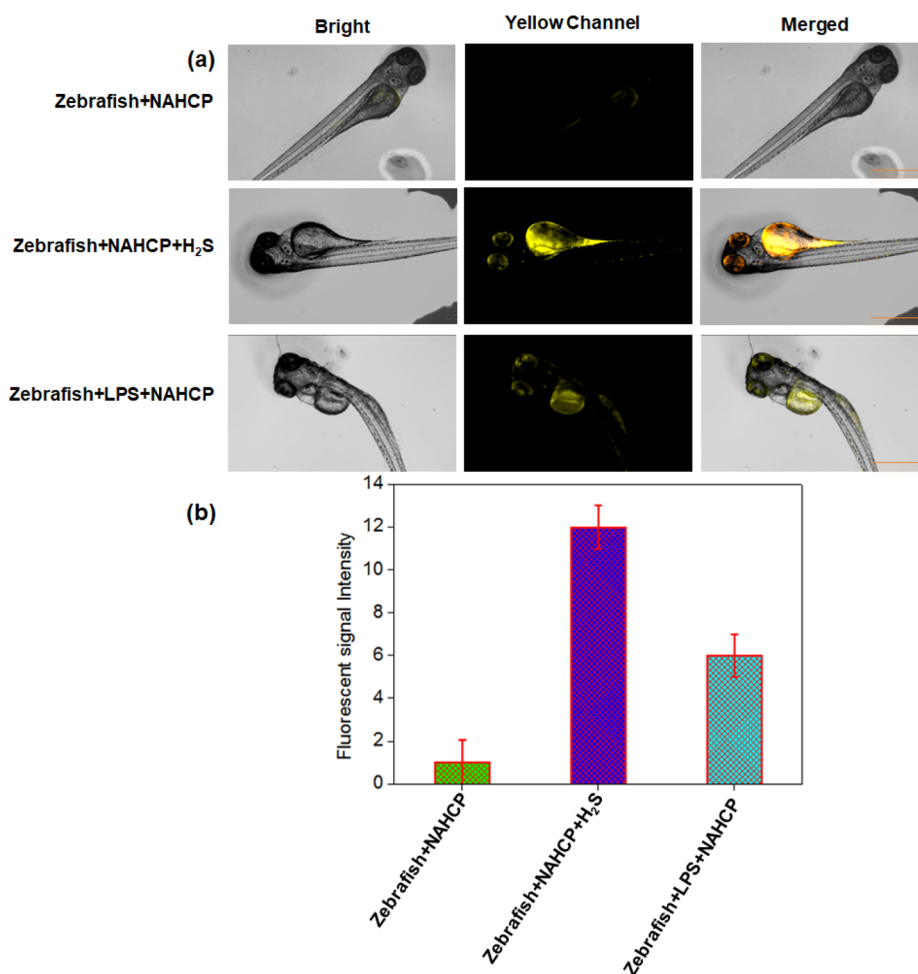

Fig. 5 (a) Fluorescence inverted microscope imaging of NAHCP (10 μM) in living zebrafish. Top row: zebrafish was incubated with NAHCP (10 μM) for 30 min as the control group; middle row: zebrafish was incubated with NAHCP (10 μM) for 30 min and then with H₂S 50 μM for 30 min; bottom row: zebrafish was incubated with LPS (1.0 μg mL⁻¹) for 2 h and then with NAHCP (10 μM) for 30 min. (b) The quantitative analysis of the average fluorescence in the top row, middle row, and bottom row. λ_{ex} = 420 nm, λ_{em} = (520−550) nm, scale bar: 10 μm, n = 3.
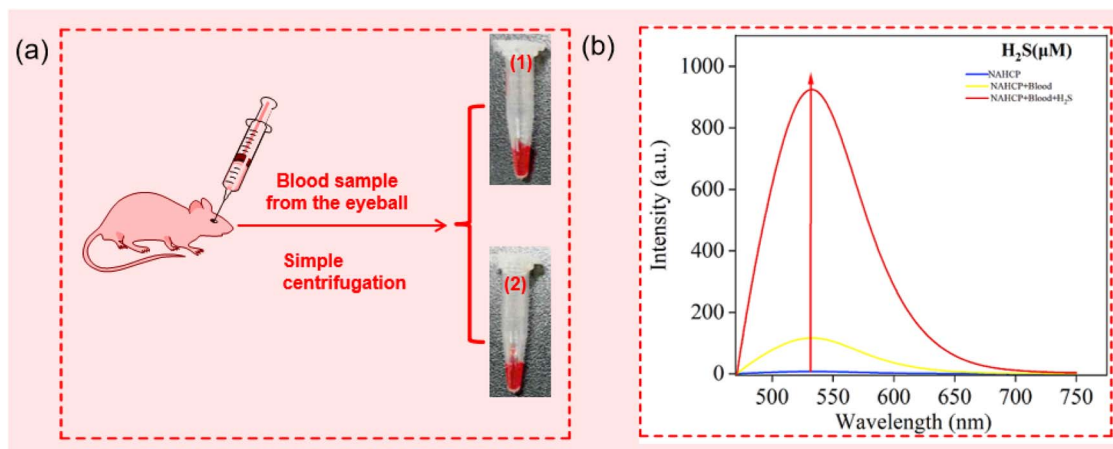
Fig. 6 NAHCP (10 μM) was applied for H$_2$S detection in blood samples (pH = 7.4, 10 mM PBS). (a) Preparation of blood samples: (1) and (2) samples were diluted with 10 mM PBS (pH = 7.4) solution, and then added and without added 100 μM H$_2$S, respectively. (b) Determine H$_2$S in blood samples with a fluorescence spectrophotometer, λ_{ex} = 420 nm, λ_{em} = 533, the λ_{ex} and λ_{em} of slits were both fixed on 5 nm, n = 3.

3.6 Detection of H$_2$S in blood samples by NAHCP

To further investigate the feasibility and practical application ability of NAHCP for H$_2$S detection in complex real samples, we detected the content of H$_2$S in mouse blood. Blood samples were obtained from the eyes of mice (Fig. 6). After simple centrifugation of the blood the serum was diluted with PBS, and then was diluted with 10 mM PBS (pH = 7.4), and then added with 100 μM H$_2$S solution or without H$_2$S solution, the samples were diluted to 5 mL with PBS to obtain the sample to be tested, and finally, the fluorescence intensity of the solution was measured with a fluorescence spectrophotometer. The experimental results showed that the fluorescence intensity of the blood with H$_2$S was higher than that without H$_2$S; the fluorescence intensities were enhanced ~17-fold and ~100-fold, respectively. Therefore, NAHCP can be applied to detect H$_2$S in complex samples and provides an effective molecular tool for rapid evaluation of the occurrence and development of diseases related to H$_2$S.

4 Conclusion

Based on the naphthylimide and 2,4-dinitrophenyl ether (rec group), a robust fluorescence "turn-on" NAHCP was constructed and applied to the specific detection and imaging analysis of H$_2$S. The o-aldehyde group and 2,4-dinitrophenyl ether group will react with H$_2$S selectively by thiolation reaction, which leads to the yellow fluorescence "turn-on", thus realizing the detection of H$_2$S. NAHCP has the advantages of high selectivity, high stability, fast response time (~2 min), and a low limit of detection 25.6 nM). Moreover, NAHCP still has superior recognition ability for H$_2$S in the presence of other biological thiols, cations, and anions, and can accurately detect H$_2$S. More importantly, NAHCP has been successfully applied in the detection and imaging research of H$_2$S in LPS-induced inflammatory biosystems. These suggest that NAHCP has the potential to become a detection and imaging analysis tool for effectively monitoring H$_2$S in complex biosystems. At the same time, it also

provides a powerful chemical tool for a deeper and comprehensive understanding of the physiological functions of H$_2$S and inflammation, a gas signaling molecule.

Ethical statement

For animal: animal welfare and experimental procedures were carried out in accordance with the guide for the care and use of laboratory animals (Ministry of Science and Technology of China, 2006), and were approved by the animal ethics committee of Central South University. *For human*: this article does not contain any studies with human participants by any of the authors.

Data availability

All relevant data are within the manuscript and its additional files.

Conflicts of interest

The authors declare no conflict of interest.

Acknowledgements

References

1 S. Jaiswal, S. P. Singh, S. Singh, R. Gupta, D. K. Tripathi, F. J. Corpas and V. P. Singh, *Plant, Cell Environ.*, 2025, **48**(3), 2445–2459.
2 F. Yuan, A. Guo, L. Wang, L. Ning, Y. Guo and J. Zhang, *Angew. Chem., Int. Ed.*, 2025, **64**(19), e202501685.

3 B. D. Paul and S. H. Snyder, *Biochem. Pharmacol.*, 2018, **149**, 101–109.

4 D. Bagal, A. Guleria, A. A. Chowdhary, P. K. Verma, S. Mishra, S. Rathore and V. Srivastava, *Physiol. Plant.*, 2025, **177**(2), e70222.

5 L. Zhou, D. Lu, Q. Wang, S. Liu, Q. Lin and H. Sun, *Biosens. Bioelectron.*, 2017, **91**, 699–705.

6 C. Munteanu, C. Popescu, A.-I. Vlădulescu-Trandafir and G. Onose, *Antioxidants*, 2024, **13**(10), 1158.

7 A. Katsouda, S.-I. Bibli, A. Pyriochou, C. Szabo and A. Papapetropoulos, *Pharmacol. Res.*, 2016, **113**(Part A), 175–185.

8 R. C. O. Zanardo, V. Brancaleone, E. Distrutti, S. Fiorucci, G. Cirino and J. L. Wallace, *FASEB J.*, 2006, **20**(12), 2118–2120.

9 U. Marcin, M. Sikora and M. Dudek, *Acta Neurobiol. Exp.*, 2008, **68**(3), 382–388.

10 A. Mironov, T. Seregina, M. Nagornykh, L. G. Luhachack, N. Korolkova, L. E. Lopes, V. Kotova, G. Zavilgelsky, Ru. Shakulov, K. Shatalin, E. Nudler and P. Natl, *Acad. Sci.*, 2017, **114**(23), 6022–6027.

11 C. K. Nicholson and J. W. Calvert, *Pharmacol. Res.*, 2010, **62**(4), 289–297.

12 E. Piragine, V. Citi, K. Lawson, V. Calderone and A. Martelli, *Biomolecules*, 2022, **12**(4), 581.

13 H. Zhao, H. Liu, Y. Yang and H. Wang, *Int. J. Mol. Sci.*, 2022, **23**(9), 4818.

14 C. Szabo, *FEBS J.*, 2020, **287**(15), 3150–3160.

15 W. Lu and J. Wen, *Mol. Neurobiol.*, 2025, 1–14.

16 H.-J. Wei, X. Li and X.-Q. Tang, *J. Clin. Neurosci.*, 2014, **21**(10), 1665–1669.

17 K. Kaleta, K. Janik, L. Rydz, M. Wróbel and H. Jurkowska, *Biomolecules*, 2024, **14**(7), 746.

18 H. M. Smith and M. D. Pluth, *JACS Au*, 2023, **3**(10), 2677–2691.

19 X. Jiang, L. Wang, S. L. Carroll, J. Chen, M. C. Wang and J. Wang, *Antioxid. Redox Signaling*, 2018, **29**(6), 518–540.

20 Y. Li, Q. Chen, X. Pan, W. Lu and J. Zhang, *Top. Curr. Chem.*, 2022, **380**(4), 22.

21 L. Yang, L. Zhou, X. Yuan, P. Lin, T. Liu, L. Chen and J. Ren, *J. Hazard. Mater.*, 2025, **484**, 136759.

22 S. Jiang, C. Xie, T. Liu, X. Yuan, J. Zheng, Z. Lian, M. Ouyang, Y. Peng and L. Zhou, *Anal. Chem.*, 2024, **96**(49), 19483–19490.

23 H. A. Henthorn and M. D. Pluth, *J. Am. Chem. Soc.*, 2015, **137**(48), 15330–15336.

24 H.-G. Wei, Y.-J. Liu and X.-D. Zhao, *Bioorg. Med. Chem. Lett.*, 2020, **30**(13), 127221.

25 S. Chen, X. Zhao and L. Zhou, *Molecules*, 2024, **29**(16), 3973.

26 R. Kaushik, R. Sakla, A. Ghosh, G. T. Selvan, P. M. Selvakumar and D. A. Jose, *ACS Sens.*, 2018, **3**(6), 1142–1148.

27 J. Hong, E. Zhou, S. Gong and G. Feng, *Dyes Pigm.*, 2019, **160**, 787–793.

28 M. Qian, L. Zhang, Z. Pu, J. Xia, L. Chen, Y. Xia, H. Cui, J. Wang and X. Peng, *J. Mater. Chem. B*, 2018, **6**, 7916–7925.

29 X. Zhao, G. Yuan, H. Ding, L. Zhou and Q. Lin, *J. Hazard. Mater.*, 2020, **381**, 120918.

30 W. Shu, L. Yan, J. Liu, Z. Wang, S. Zhang, C. Tang, C. Liu, B. Zhu and B. Du, *Ind. Eng. Chem. Res.*, 2015, **54**(33), 8056–8062.

31 C. Xie, Y. Peng, Z. Zhang, K. Luo, Q. Yang, L. Tan and L. Zhou, *Anal. Chem.*, 2024, **96**, 5006–5013.

32 L. Kong, Q. Bai, C. Li, Q. Wang, Y. Wang, X. Shao, Y. Wei, J. Sun, Z. Yu, J. Yin, B. Shi, H. Fang, X. Chen and Q. Chen, *Nat. Commun.*, 2024, **15**(1), 9413.

33 W. Hao, D. Wu, X. Huang, A. Huang, H. Xu, Z. Xia, Y. Liang and H. He, *Chem. Phys. Lett.*, 2025, **861**, 141845.

34 C. Zhang, Yi. Wang, X. Li, C. Liu, S. Nie, Y. Li and C. Liu, *Tetrahedron Lett.*, 2022, **110**, 154199.